***Proceedings of the IASS 2024 Symposium***
*Redefining the Art of Structural Design*
August 26-30, 2024, Zurich Switzerland
Philippe Block, Giulia Boller, Catherine DeWolf,
Jacqueline Pauli, Walter Kaufmann (eds.)

# Counting-up and classification of all combination patterns of singular generalized Miura-ori

Hiroyuki TAGAWA*, Ayumi SUGIMURA[a], Ayana MUKAI, Keisuke INOMATA

*Mukogawa Women's University
1-13 Tozaki-cho, Nishinomiya, Hyogo, 663-8121, JAPAN
tagawa@mukogawa-u.ac.jp

[a] Shimizu Corporation

## Abstract

An arc- and spiral-shaped Miura-ori, which is rigid-flat-foldable and a type of singular generalized Miura-ori, was proposed in a previous study. This study conducts the counting and classification of all combination patterns of the singular generalized Miura-ori, which is defined as the generalized Miura-ori that has symmetry and regularity in included angles to enable rigid flat-foldability, in a 3 × 3 quadrilateral mesh unit with looped 4 nodes. The study discovered a total of 26 patterns of singular generalized Miura-ori in the canonical arrangement distributed as follows: 11 patterns for $K_1$=$K_4$, $K_2$=$K_3$, 11 patterns for $K_1$=$K_2$, $K_3$=$K_4$, and four patterns for $K_1$=$K_2$=$K_3$=$K_4$, where $K$ denotes the conversion coefficient. For example, the conventional Miura-ori is classified as $K_1$=$K_2$=$K_3$=$K_4$ and the arc- and spiral-shaped Miura-ori are classified as $K_1$=$K_2$, $K_3$=$K_4$. Among the singular generalized Miura-ori, the arc- and spiral-shaped Miura-ori are the only patterns in which all the fold lines are not parallel to each other and change direction with a constant angle at the intersections. Furthermore, each of the 26 patterns can be repeated in the horizontal and vertical directions to generate tessellation. Finally, the study showcases several examples of how singular generalized Miura-ori, including arc- and spiral-shaped Miura-ori, can be applied to the design proposal of roof architectures. These applications demonstrate the versatility of such structures, which are deployable, foldable, or fixed as needed in architectural and engineering contexts.

**Keywords**: Singular generalized Miura-ori, arc- and spiral-shaped Miura-ori, origami, rigid-flat-foldable, deployable, counting-up, large roof architecture

## 1. Introduction

Miura-ori [1] is a method of folding a flat surface, such as a sheet of paper, into a smaller area. Miura-ori crease patterns form a tessellation of a surface composed of repeating parallelograms with alternating mountain and valley fold lines. Miura-ori is a form of rigid-foldable quadrilateral mesh origami that enables continuous rigid motion with one degree of freedom while keeping each facet flat. Miura-ori is popular as the most efficient crease pattern and has been applied in various engineering fields, such as deployable solar panels for use in space or folding maps.

Recently, researchers have proposed systematic ([2], [3]), freedom [4], and variations of the Miura pattern. Tachi [4] proposed a generalization of–d the foldable quadrilateral mesh origami. Geometric conditions for enabling rigid motion in general quadrilateral mesh origami without trivial repeating symmetry were derived. Additionally, Tachi [5] provided single-curvature Miura-ori and Mars folding [6] as examples of trivial models of generalized Miura-ori. Under these conditions, Tachi [5]

demonstrated a method to explore freeform variations of the generalized Miura-ori using a rigid origami simulator.

In a previous study [7], we proposed an arc- and spiral-shaped Miura-ori in which quadrilaterals with identical internal angles were arrayed in the same column to enable the deployment mechanism. In this study investigates the enumeration and classification of all combination patterns of a singular generalized Miura-ori in a canonical arrangement. We explore the geometric configurations of the included angle-combination patterns, with particular attention to the unique features of the spiral Miura-ori. Additionally, we examine the geometric generation of tessellation by repeatedly employing the same combination pattern. Finally, we showcase instances of applying both arc- and spiral-shaped Miura-ori as singular generalized Miura-ori in architectural and structural roof design.

## 2. Generalized Miura-ori and singular generalized Miura-ori

### 2.1. Generalized Miura-ori

The deployment angles are related to the angles between the fold lines around one node, as shown in Figure 1, and are given by Equations (1) and (2), where $K$ is the conversion coefficient given by Equation (3) and is defined by Tachi [4]. It should be noted that angles $\theta_i$ and $\theta_j$ are commutative for the same $K$ value. For the looped 4 nodes, as shown in Figure 2, the deployment angles $\rho_1$, $\rho_2$, $\rho_3$, $\rho_4$, and $\rho_5$ are related using Equations (4), (5), (6), and (7). If linked rigid-folding behavior is realized, as shown in Figure 3, Equation (8) should be satisfied. Therefore, Equation (9) is satisfied for any $\rho_1$. This results in Equation (10): This equation was derived from Tachi [4] using different notation.

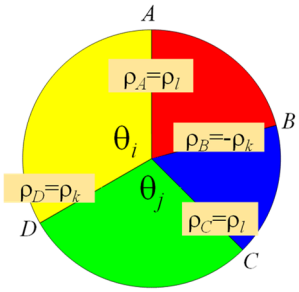


Figure 1: Disk with 1 node and 4 lines

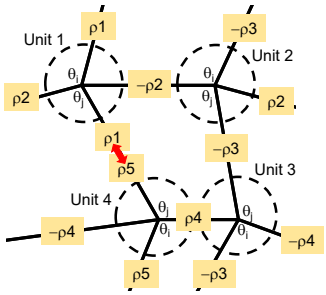


Figure 2: Loop with 4 nodes

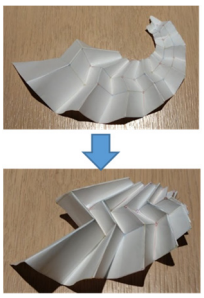

Figure 3: Linked rigid flat-folding

$$\cos\rho_k = K + \frac{1-K^2}{\cos\rho_l + K} \quad (1) \qquad \cos\rho_l = -K + \frac{1-K^2}{\cos\rho_k - K} \quad (2)$$

$$K = \frac{1+\cos\theta_i\cos\theta_j}{\sin\theta_i\sin\theta_j} \quad (3)$$

$$\cos\rho_2 = K_1 + \frac{1-K_1^2}{\cos\rho_1 + K_1} \quad (4) \qquad \cos\rho_3 = -K_2 + \frac{1-K_2^2}{\cos\rho_2 - K_2} \quad (5)$$

$$\cos\rho_4 = K_3 + \frac{1-K_3^2}{\cos\rho_3 + K_3} \quad (6) \qquad \cos\rho_5 = -K_4 + \frac{1-K_4^2}{\cos\rho_4 - K_4} \quad (7)$$

$$\cos\rho_5 = \cos\rho_1 \quad (8)$$

$$\frac{1-K_3^2}{\frac{1-K_4^2}{\cos\rho_1 + K_4} + K_4 - K_3} - K_3 = \frac{1-K_2^2}{\frac{1-K_1^2}{\cos\rho_1 + K_1} + K_1 - K_2} - K_2 \quad (9)$$

$$(K_4 - K_3)(1 - K_1K_2) = (K_1 - K_2)(1 - K_3K_4) \quad (10)$$

An example of the generalized Miura-ori for 4 × 4 panels, in which the angles at the intersections between the fold lines are random except when satisfying Equation (10), is shown in Figure 4. Here, $K_1 \neq K_2 \neq K_3 \neq K_4$. Simulation results for the rigid flat-folding behavior are shown in Figure 4.

| unit | $\theta_i$(°) | $\theta_j$(°) | $K$ |
|---|---|---|---|
| 1 | 122.28 | 113.97 | 1.575 |
| 2 | 121.97 | 117.24 | 1.647 |
| 3 | 122.37 | 117.19 | 1.657 |
| 4 | 108.52 | 127.41 | 1.584 |

| unit | $\theta_i$(°) | $\theta_j$(°) | $K$ |
|---|---|---|---|
| 5 | 126.05 | 116.12 | 1.735 |
| 2 | 121.97 | 117.24 | 1.647 |
| 3 | 122.37 | 117.19 | 1.657 |
| 6 | 111.35 | 130.51 | 1.746 |

| unit | $\theta_i$(°) | $\theta_j$(°) | $K$ |
|---|---|---|---|
| 4 | 108.52 | 127.41 | 1.584 |
| 3 | 122.37 | 117.19 | 1.657 |
| 8 | 108.45 | 131.55 | 1.704 |
| 9 | 135.55 | 99.77 | 1.625 |

| unit | $\theta_i$(°) | $\theta_j$(°) | $K$ |
|---|---|---|---|
| 3 | 122.37 | 117.19 | 1.657 |
| 6 | 111.35 | 130.51 | 1.746 |
| 7 | 139.69 | 100.93 | 1.802 |
| 8 | 108.45 | 131.55 | 1.704 |

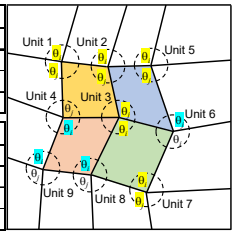


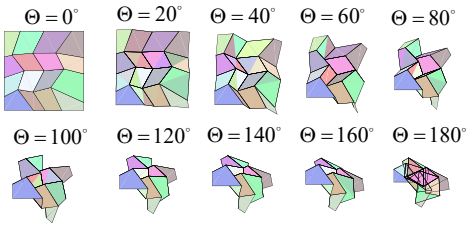


Figure 4: Example of generalized Miura-ori

## 2.2. Singular generalized Miura-ori

The singular generalized Miura-ori, as defined in this study, refers to the generalized Miura-ori characterized by symmetry and regularity in the combination of included angles at intersections. It falls under either of the cases specified by Equations (11), (12), and (13).

$$K_1 = K_4, \quad K_2 = K_3 \tag{11}$$

$$K_1 = K_2, \quad K_3 = K_4 \tag{12}$$

$$K_1 = K_2 = K_3 = K_4 \tag{13}$$

## 2.3. Canonical and noncanonical arrangements

The canonical arrangement, which was considered in this study, and the noncanonical arrangement are shown in Figure 5. The arc-shaped Miura-ori, as an example of the canonical arrangement, and the oval tessellation, as an example of the noncanonical arrangement, are shown in Figures 6 and 7, respectively.

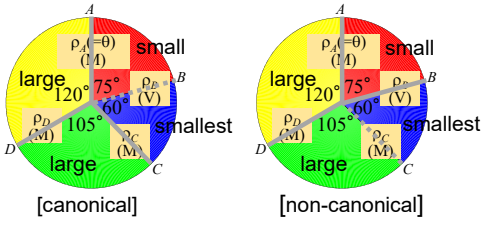


(a) Mountain-valley fold lines

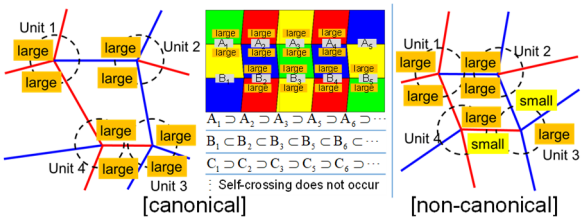


(b) Large ( $\geq 90^\circ$ ) and small ( $< 90^\circ$ ) angles

Figure 5: Canonical and noncanonical arrangements (left: canonical, right: noncanonical)

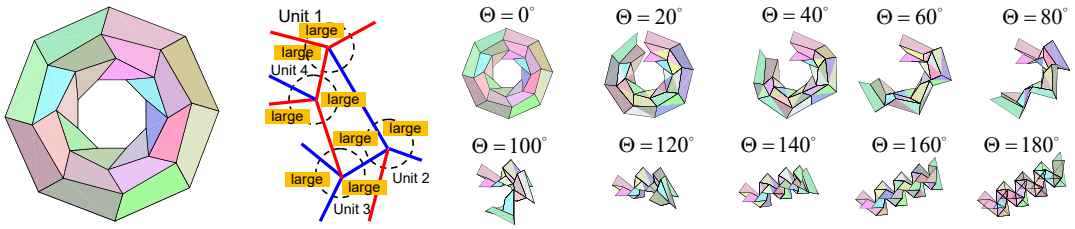


Figure 6: Arc-shaped Miura-ori (canonical arrangement)

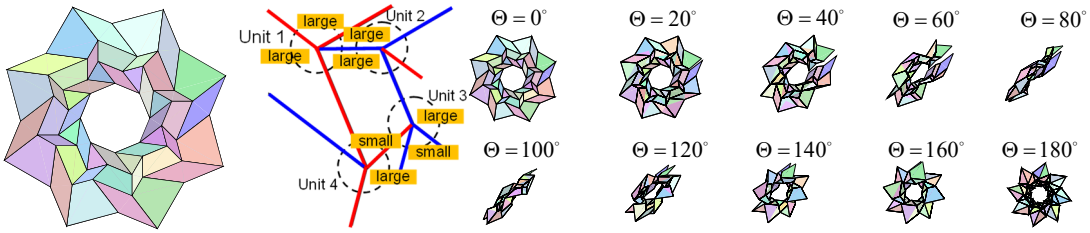


Figure 7: Oval tessellation (noncanonical arrangement)

## 3. Counting-up and classification of singular generalized Miura-ori

### 3.1. Counting-up of singular generalized Miura-ori

The enumeration of singular generalized Miura-ori in the canonical arrangement is performed for each case that satisfies Equations (13), (14), and (15).

#### *3.1.1. Case of $K_1$=$K_4$, $K_2$=$K_3$*

All possible patterns for $K_1$=$K_4$ and $K_2$=$K_3$, including the insistent and overlapping patterns that are eliminated later, are shown in Figure 8. There are 9 patterns with 2 kinds of angles (●, □), 20 patterns with 3 kinds of angles (●, □, △), and 4 patterns with 4 kinds of angles (●, □, △, ◆), totaling 33 patterns.

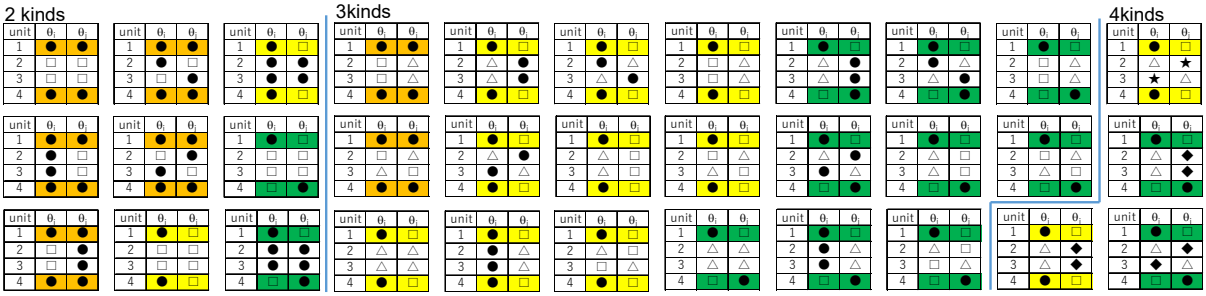


Figure 8: All possible patterns including inconsistent and overlapped patterns

The sum of the four internal angles of a quadrilateral is 360°. Therefore, the internal angles shown in Figure 9 should adhere to Equation (16). An example of an inconsistent pattern is shown in Figure 10. In this scenario, the pattern is categorized with two types of included angles (●, □). To satisfy Equation (15), ● must equal □. Consequently, this pattern is counted as having only one type. The process used to assess consistency and eliminate inconsistent patterns is illustrated in Figure 11. Eighteen patterns (×) were eliminated due to inconsistency. The remaining 12 patterns (◎) satisfy Equation (15) unconditionally. The 3 patterns (○) satisfy Equation (14) subject to the conditions on ★ colored in green, as shown in Figure 11. Consequently, the number of possible patterns decreased from 33 to 15.

$$\left(360^\circ-\theta_i^1\right)+\theta_j^2+\left(360^\circ-\theta_i^3\right)+\theta_j^4=360^\circ \qquad \therefore \theta_i^1+\theta_i^3=\theta_j^2+\theta_j^4 \tag{14}$$

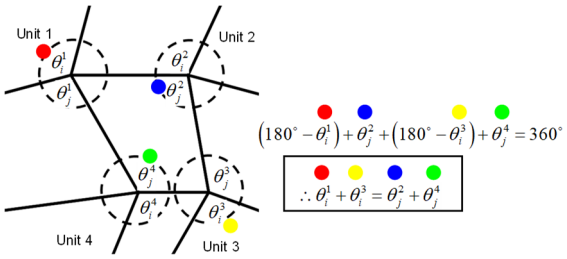


Figure 9: Consistent condition

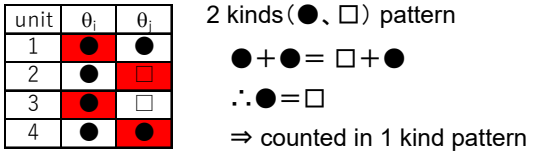


Figure 10: Example of inconsistent pattern

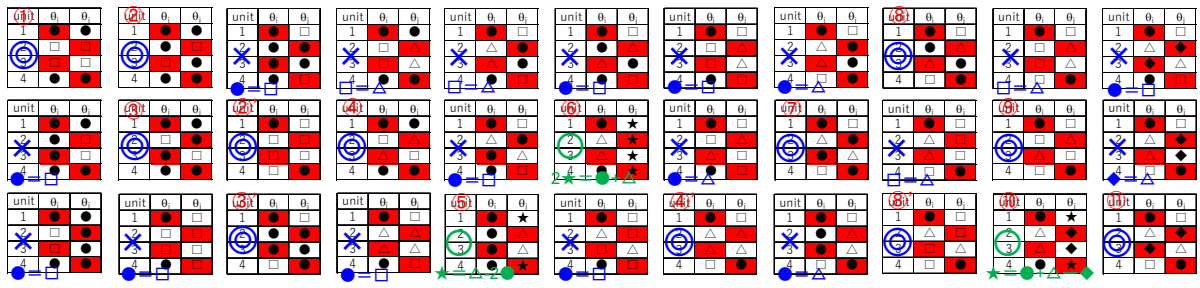

Figure 11: Assessing consistency and excluding inconsistent patterns

Furthermore, overlapping patterns were eliminated. Two examples of overlapping patterns are shown in Figure 12. The pattern ③ was rotated by 180°, which is identical to pattern ③'. Pattern ② is rotated by 180° and the marker is changed between □ and ●, which is identical to Pattern ②'. Thus, seven patterns were identical to themselves after a 180° rotation, and four patterns were identical to the other four patterns, as shown in Figure 13. The number of possible patterns decreased from 15 to 11. All 11 combination patterns for $K_1$=$K_4$, $K_2$=$K_3$ are shown in Figure 14.

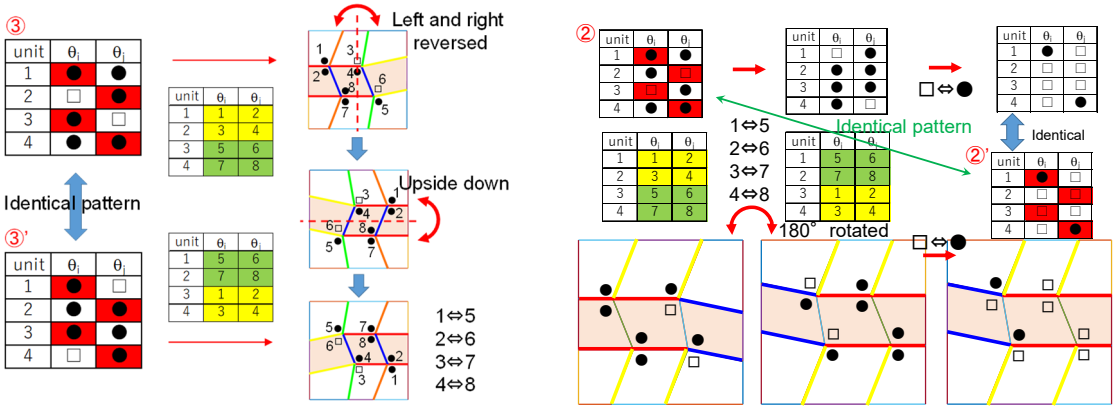


Figure 12: Examples of overlapped patterns

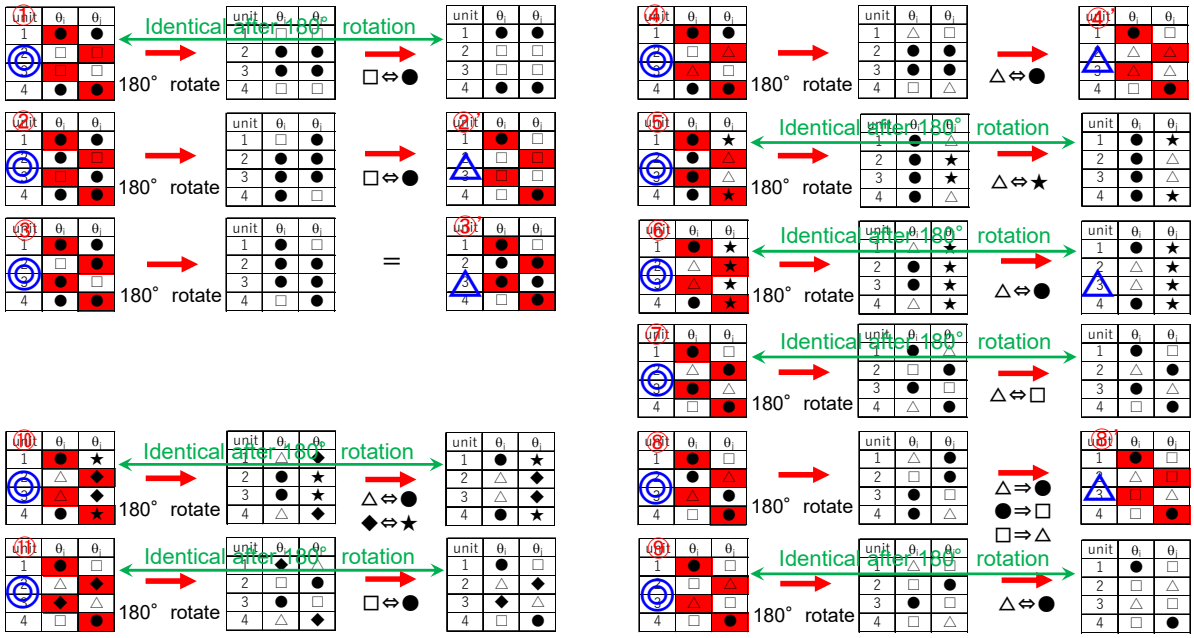


Figure 13: Identifying overlapped patterns

All possible 11 patterns for $K_1$=$K_4$ and $K_2$=$K_3$ are summarized in Figure 13.

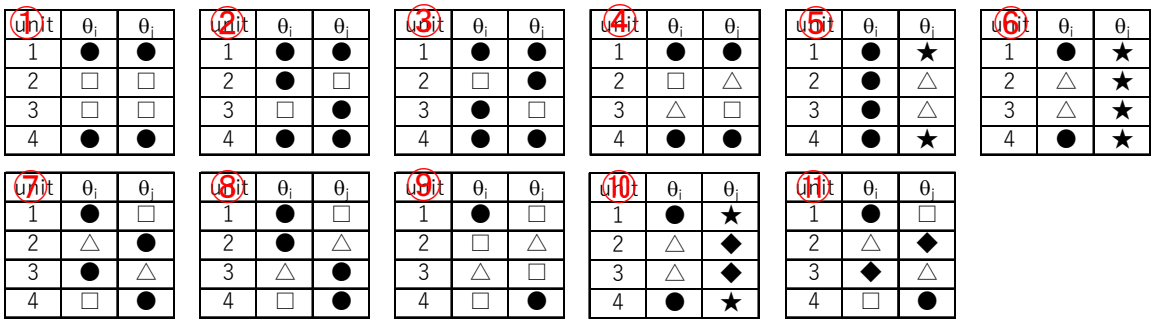

Figure 14: 11 combination patterns for the case of $K_1$=$K_4$, $K_2$=$K_3$

### *3.1.2. Case of $K_1$=$K_2$, $K_3$=$K_4$*

The patterns for the cases of $K_1$=$K_2$, $K_3$=$K_4$ are obtained by changing the columns corresponding to units 2 and 4 in the cases of $K_1$=$K_4$, $K_2$=$K_3$ because the procedures to eliminate the inconsistent and overlapped patterns are the same. All 11 patterns for $K_1$=$K_2$, $K_3$=$K_4$ are shown in Figure 15.

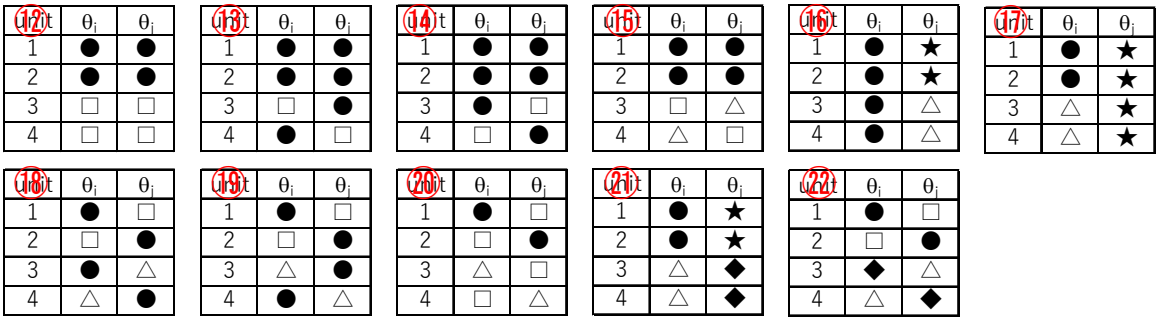

Figure 15: 11 combination patterns for the case of $K_1$=$K_2$, $K_3$=$K_4$

### *3.1.3. Case of $K_1$=$K_2$=$K_3$=$K_4$*

All possible patterns for the case of $K_1$=$K_2$=$K_3$=$K_4$, including the insistent and overlapping patterns that were eliminated later, are shown in Figure 16. There is 1 pattern with one kind of an angle (●) and 8 patterns with 2 kinds of angles (●, □). In total, there are 9 patterns.

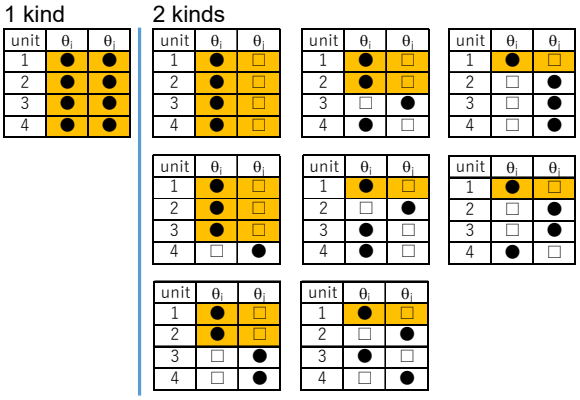


Figure 16: All possible patterns including inconsistent and overlapped patterns

The process of evaluating the consistency and eliminating inconsistent patterns is shown in Figure 17. The number of combination patterns decreased from nine to four. The process used to evaluate overlapping patterns is illustrated in Figure 18. All four patterns were identical to themselves after 180° rotation, and there were no overlapping patterns.

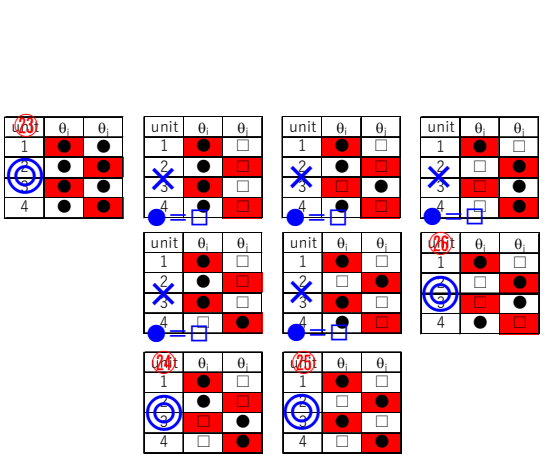

Figure 17: Excluding inconsistent patterns

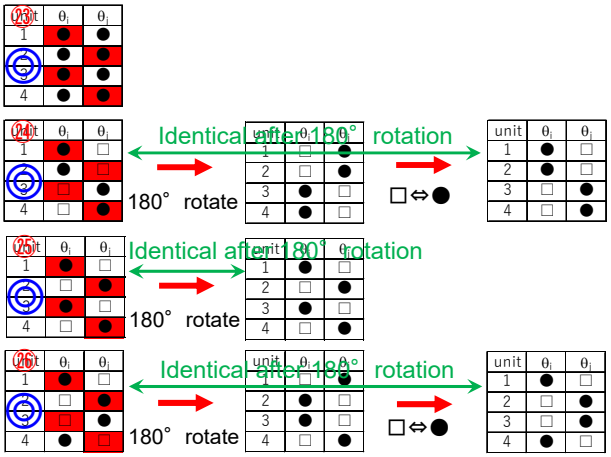


Figure 18: Identifying overlapped patterns

All four patterns for $K_1$=$K_2$=$K_3$=$K_4$ are summarized in Figure 19.

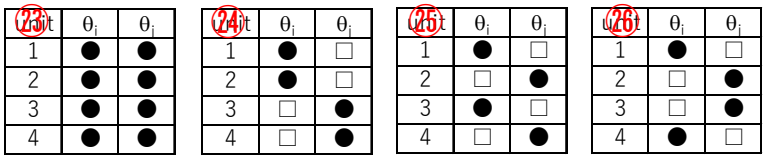


Figure 19: Four combination patterns for the case of $K_1$=$K_2$=$K_3$=$K_4$

The total number of combination patterns for the singular generalized Miura-ori is 26, in which 11 patterns are for the cases of $K_1$=$K_4$, $K_2$=$K_3$ as shown in Figure 14; 11 patterns are for the cases of $K_1$=$K_2$, $K_3$=$K_4$, as shown in Figure 15; and four patterns are for the cases of $K_1$=$K_2$=$K_3$=$K_4$, as shown in Figure 19.

### 3.2. Geometric configurations corresponding to 26 patterns

The geometric configurations corresponding to the 26 combination patterns are shown in Figure 20. Thick lines with the same color represent fold lines parallel to each other, owing to the symmetric and regular combination patterns. Single-curvature Miura-ori is ①, spiral-shaped Miura-ori is ㉑, Miura-ori is ㉓, and Mars folding [6] is patterns ㉖. Among the 26 patterns, the spiral-shaped Miura-ori is the only one that did not have parallel fold lines.

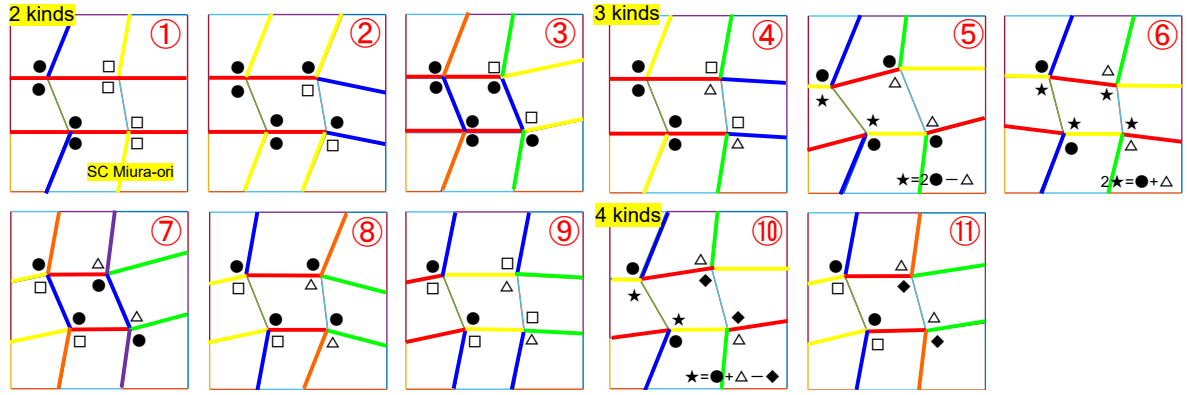


(a) Case of $K_1$=$K_4$, $K_2$=$K_3$

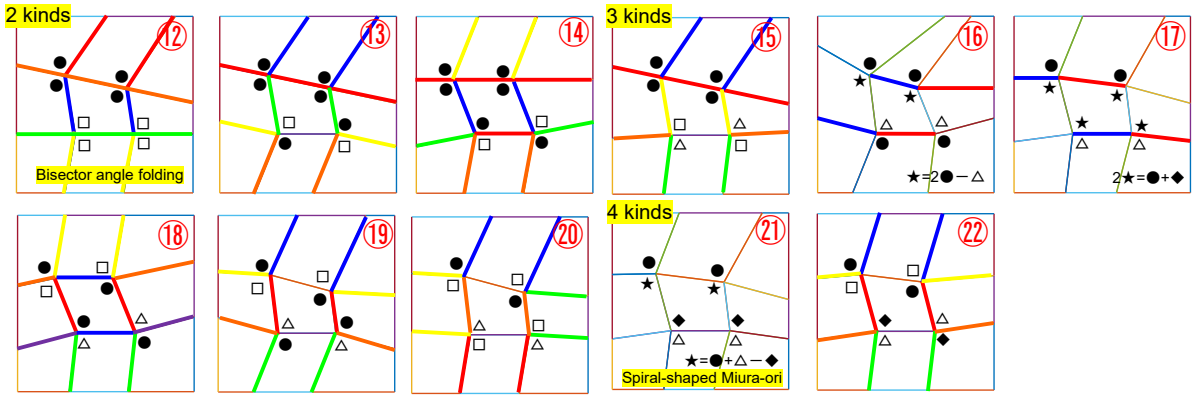


(b) Case of $K_1$=$K_2$, $K_3$=$K_4$

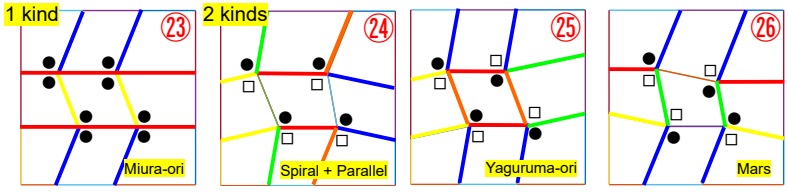


(c) Case of $K_1$=$K_2$=$K_3$=$K_4$

Figure 20: Geometric configurations corresponding to 26 combination patterns

## 4. Tessellation repeating same patterns of singular generalized Miura-ori

The tessellation generated by repeating the same patterns as the singular generalized Miura-ori was considered, as shown in Figure 21. Extensions in the horizontal and vertical directions were examined, as shown in Figure 22. If two lines in the same array are parallel on the right and left sides, such as in pattern ⑨, then the same pattern can be extended horizontally. Similarly, if two lines in the same column are parallel on the top and bottom sides, as in Pattern ⑩, the same pattern can be extended vertically. If the lines on the right and left sides are not parallel, as in pattern ⑯, the same pattern can still be extended owing to the condition of the included angles. As a result, tessellations were possible for all 26 patterns in both the horizontal and vertical directions. As examples, the tessellations of patterns ①, ㉒ and ㉖ are shown in Figure 23. Although the quadrilateral mesh is sometimes distorted, 5 × 5 tessellations can be generated by repeating each of the 26 patterns in at least one of the two combinations of included angles, as shown in Figure 24.

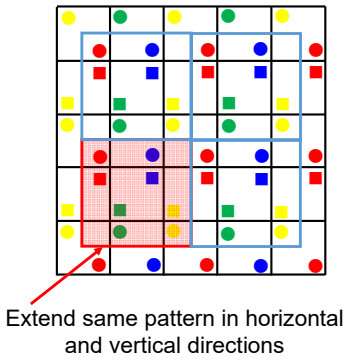


Figure 21: Tessellation by repeating same pattern

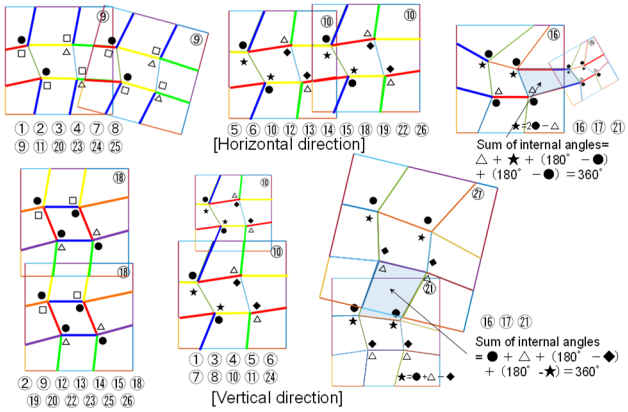


Figure 22: Extension of same pattern

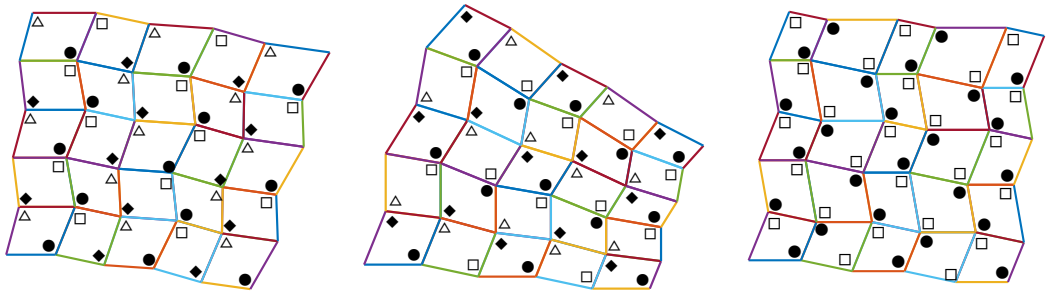

(a) Pattern ① (b) Pattern ㉒ (c) Pattern ㉖ (Mars)

Figure 23: Examples of tessellation by repeating same pattern

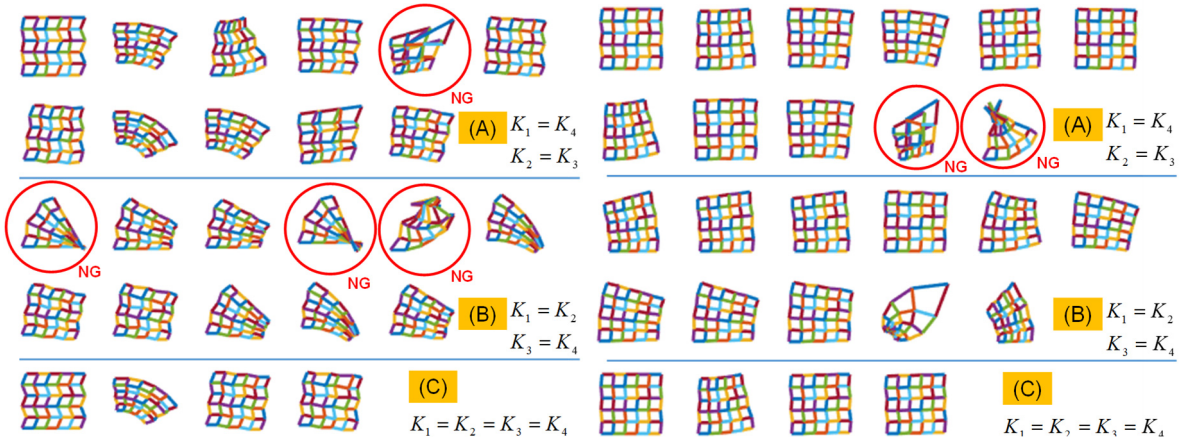


(a) ●=112°,□=100°, ◆=97°, △=105° (b) ●=95°,□=98°, ◆=91°, △=118°

Figure 24: 5 × 5 tessellations generated by repeating each of the 26 combination patterns

## 5. Application of arc- and spiral-shaped Miura-ori to large roof architecture

The large roof structure obtained by the proposed arc-shaped and spiral-shaped Miura-ori has an elegant and natural shape with sharp mountain-valley lines. Design examples of the application of arc-shaped and spiral-shaped Miura-ori to roof architecture are demonstrated.

### 5.1. Application of arc-shaped Miura-ori

A large-roof architecture with an arc-shaped Miura-ori was proposed, as shown in Figure 25. The enclosed configuration obtained by iterations in the rigid flat-folding numerical simulation [7] was self-balanced. The enclosed arc-shaped Miura-ori wooden roof with outer diameter of 50 m and panel thickness of 0.15 m is analyzed for gravity loading. The panels were modeled using plate elements. One-directional rotation along the fold lines was modeled by separate nodes at the same coordinates along the fold lines provided by the multiple-point constraint, as shown in Figure 26. The vertex node was modeled using a pin. If the inner nodes are not supported, then the structure is highly flexible. If both the outer and inner nodes are pin supported, the von Mises stresses and deflections are small, as shown in Figure 27.

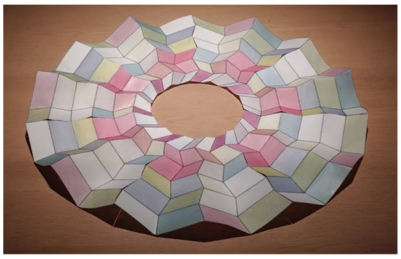

Figure 25: Arc-shaped Miura-ori

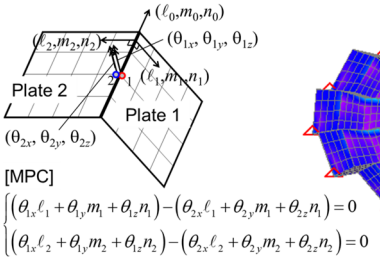


Figure 26: Modeling of fold line

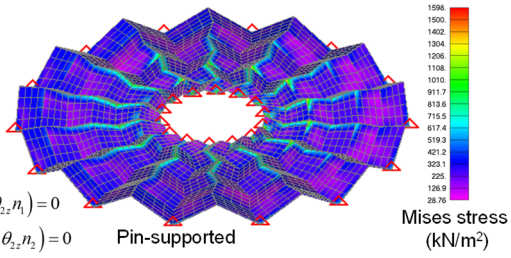


Figure 27: Analysis results

### 5.2. Application of spiral-shaped Miura-ori

The included angle $\alpha_3$ in the arc- and spiral-shaped Miura-ori is calculated using Equation (15), given $r$, $d$, $\alpha_1$, $\alpha_2$ and the magnification factor $\phi$, as shown in Figure 28. If $\phi$=1.0, the configuration of the arc-shaped Miura-ori is obtained. If $\phi$>1.0, a spiral-shaped Miura-ori is obtained. The geometric configurations of the arc-shaped and spiral-shaped Miura-ori were controlled by the value of $\phi$, as shown in Figure 29. The architectural and structural design of a hybrid structure composed of a suspended spiral-shaped Miura-ori roof and twin towers for a hiker's rest station on Mt. Rokko was proposed, as shown in Figure 30.

$$\alpha_3 = \arccos\left(\frac{r\cos\alpha_1\cdot\left(r\cos\alpha_1+\phi r\cos\alpha_2-d\right)+r\sin\alpha_1\left(r\sin\alpha_1-\phi r\sin\alpha_2\right)}{\sqrt{\left(d-r\cos\alpha_1-\phi r\cos\alpha_2\right)^2+\left(r\sin\alpha_1-\phi r\sin\alpha_2\right)^2}}\right) \tag{15}$$

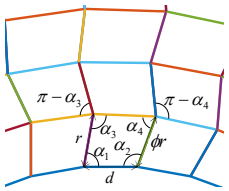


Figure 28: Generation of arc- and spiral-shaped Miura-ori

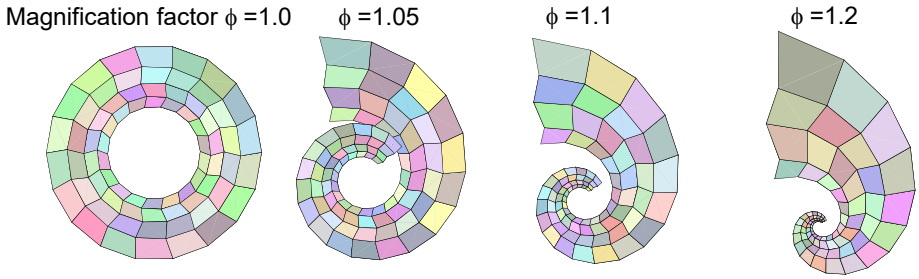


Figure 29: Configurations of arc- and spiral-shaped Miura-ori controlled by the magnification factor $\phi$

Figure 30: Design proposal: hybrid structure with spiral-shaped Miura-ori roof and twin towers

## 6. Conclusion

In this study, the counting-up and classification of possible combination patterns of singular generalized Miura-ori were conducted. Major findings include:

1) There are 26 singular generalized Miura-ori patterns in the canonical arrangement.
2) Spiral-shaped Miura-ori is the only pattern in which all the fold lines are not parallel to each other and change direction with a constant angle at the intersections.
3) Tessellation was generated by repeating each of the 26 patterns in both horizontal and vertical directions.

## Acknowledgments

This work was supported by the JSPS Grants in Aid for Scientific Research (grant numbers JP23K04113 and JST CREST JPMJCR1911).

## References

[1] K. Miura, "Method of packaging and deployment of large membranes in space," *Institute of Space and Astronautical Science*, Report No. 618, 1985.

[2] T. Nojima, "Modelling of folding patterns in flat membranes and cylinders by origami," *JSME International Journal Series C*, Vol. 45, No. 1, 2002.

[3] P. Sareh and S. D. Guest, "Tessellating variations on the Miura fold pattern," *IASS-APCS Symposium*, Seoul, South Korea, 2012.

[4] T. Tachi, "Generalization of rigid foldable quadrilateral mesh origami," *Proceedings of the IASS symposium 2009*, Valencia, Spain, 2009.

[5] T. Tachi, "Rigid origami simulator," 2007, http://www.tsg.ne.jp/TT/software/.

[6] P. T. Barreto, 'Lines meeting on a surface: the "mars' paperfolding, *Origami Science & Art, Proceedings of the 2nd international meeting of Origami science and scientific Origami*, 1997.

[7] H. Tagawa, N. Yoshioka, T. Suzuki, "Proposal of arc- and spiral-shaped Miura-ori and its application to the design of large roof architecture," *Proceedings of the IASS symposium 2022*, Beijing, China, 2022.